analytical chemistry

Article

pubs.acs.org/ac

Assessment of Binding Affinity between Drugs and Human Serum Albumin Using Nanoporous Anodic Alumina Photonic Crystals

Mahdieh Nemati, Abel Santos,* Cheryl Suwen Law, and Dusan Losic*

School of Chemical Engineering, The University of Adelaide, Engineering North Building, 5005 Adelaide, Australia

Supporting Information

ABSTRACT: In this study, we report an innovative approach aiming to assess the binding affinity between drug molecules and human serum albumin by combining nanoporous anodic alumina rugate filters (NAA-RFs) modified with human serum albumin (HSA) and reflectometric interference spectroscopy (RIfS). NAA-RFs are photonic crystal structures produced by sinusoidal pulse anodization of aluminum that present two characteristic optical parameters, the characteristic reflection peak (λ_{Peak}), and the effective optical thickness of the film (OT_{eff}), which can be readily used as sensing parameters. A design of experiments strategy and an ANOVA analysis are used to establish the effect of the anodization parameters (i.e., anodization period and anodization offset) on the sensitivity of HSA-modified NAA-RFs toward indomethacin, a model drug. To this end, two sensing parameters are used, that is, shifts in the characteristic reflection peak ($\Delta\lambda_{Peak}$) and changes in the effective optical thickness of the film (ΔOT_{eff}). Subsequently, optimized NAA-RFs are used as sensing platforms to determine the binding affinity between a set of drugs (i.e., indomethacin, coumarin, sulfadymethoxine, warfarin, and salicylic acid) and HSA molecules. Our results verify that the combination of HSA-modified NAA-RFs with RIfS can be used as a portable, low-cost, and simple system for establishing the binding affinity between drugs and plasma proteins, which is a critical factor to develop efficient medicines for treating a broad range of diseases and medical conditions.

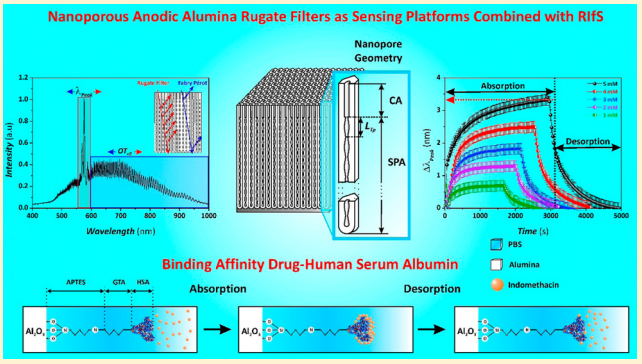

In the past decade, the discovery of new drugs and therapeutic agents has yielded outstanding improvements in quality of life, health, and life expectancy.[1,2] These significant advancements made by pharmaceutical research and innovation have resulted in drug discoveries that can address or minimize the effects associated with a broad range of diseases and medical conditions, including chronic pain, arthritis, cancer, metabolic and gastrointestinal disorders, infectious and cardiovascular diseases, and mental disorders.[3,4] One key factor playing a critical role in this innovation-driven progress is to understand the underlying mechanisms in drug efficacy and failure. For instance, pharmacokinetics (i.e., the fate of substances administered externally to a living organism) of drugs and medicaments is a critical aspect to take into account in the design of effective therapeutics.[5,6] Most of the drugs bind reversibly to plasma proteins present in the serum and blood such as glycoprotein and human serum albumin (HSA). Therefore, the affinity of medicaments toward these proteins is of critical importance to determine the overall pharmacokinetic profile of any therapeutic substance. Clinical patients present different levels of these proteins, which in turn makes the free concentration of drug patient-dependent. As a result, the therapeutic effect of medicaments with high affinity toward these circulating proteins could have a significant variance as a function of the levels of these biomolecules. This phenomenon can also extend the activity of a given drug for a longer time period given that the complexes formed between medicaments and proteins can replenish the concentration of free drug as this is removed from the body. Hence, establishment of the affinity between drugs and circulating proteins is a critical factor to consider in the design and assessment of medicines.

Although the drug−protein affinity should be established on a patient-by-patient basis using serum or blood samples, some analytical techniques can provide an accurate estimation of this binding affinity by using simple molecules such as HSA. These simplified analyses can be readily used to design more effective therapeutics in a time-effective and cost-competitive manner, when many compounds must be screened. Some of these analytical methods have been extensively used by pharmaceutical industry, including ultrafiltration, centrifugation, size exclusion and affinity chromatography, dialysis, spectroscopy, electrophoresis, and surface plasmon resonance (SPR).[7−9] Most of these analytical techniques are based on changes in intrinsic parameters of molecules and complexes (e.g., spectroscopic signature, mobility, charge, etc.) or on separation processes. Among the different alternative techniques, reflectometric interference spectroscopy (RIfS) has demonstrated

Received: March 12, 2016
Accepted: April 29, 2016

DOI: 10.1021/acs.analchem.6b00993
Anal. Chem. XXXX, XXX, XXX−XXX

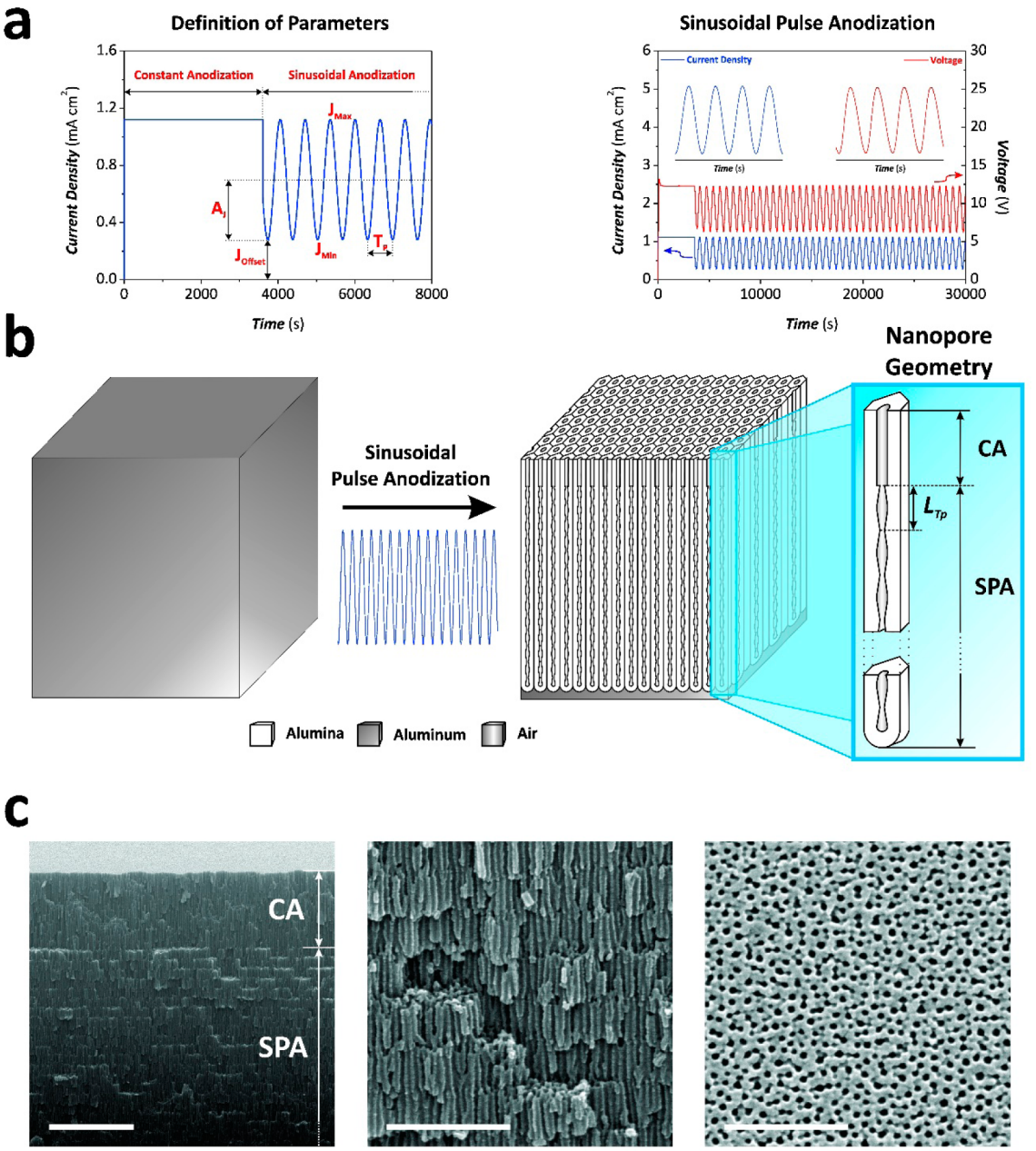

Figure 1. Concept of sinusoidal pulse anodization approach used to produce nanoporous anodic alumina rugate filters. (a) Example of sinusoidal anodization wave with T_P = 750 s used to fabricate NAA-RFs (left, definition of anodization parameters: T_P = anodization period, A_J = anodization amplitude, J_{Offset} = anodization offset, J_{Max} = current density maximum, and J_{Min} = current density minimum; left, example of anodization profile with insets showing details of the current density and voltage profiles). (b) Schematic illustration of the conversion of aluminum substrates into NAA-RFs by sinusoidal pulse anodization and graphical definition of period length (L_{Tp}). (c) Representative cross-section and top view SEM images of NAA-RFs produced by sinusoidal pulse anodization approach [left, general cross-section view SEM image of a NAA-RF produced with T_p = 750 s, A_J = 0.42 mA cm^{-2}, J_{Offset} = 0.28 mA cm^{-2}, N_P = 150 pulses, T_{An} = −1 °C, and t_{pw} = 6 min (scale bar = 2 μm), where CA and SPA denote the layers produced at constant and sinusoidal pulse anodization modes, respectively; center, magnified view of part a (scale bar = 500 nm); right, top view SEM image of a NAA-RF (scale bar = 250 nm)].

outstanding capabilities and versatility for different sensing applications.[10,11] RIfS is a label-free optical sensing technique that relies upon the multiple reflection of white light at the interfaces of solid thin films.[12,13] As a result of this light−matter interaction, constructive and destructive interferences of the reflected light form a characteristic interference pattern by the Fabry−Pérot effect.[14,15] These interferences can be used as sensing principle to detect analytes of interest in real-time, with precision. The analytical use of RIfS was pioneered by Gauglitz and co-workers, who used solid films based on glass and biopolymers with a sensitive layer (i.e., layer where the binding events between analyte and capturing molecules occur).[16] Sailor and co-workers exploited the combination of RIfS with porous silicon photonic crystals, which are photonic structures that can guide, reflect, confine, and transmit light in a selective manner by engineering their nanoporous structure.[17,18] Recently, we have also demonstrated and exploited the combination of RIfS with nanoporous anodic alumina (NAA) photonic crystals, which are produced by electrochemical oxidation (i.e., anodization) of aluminum substrates.[19−24]

DOI: 10.1021/acs.analchem.6b00993
Anal. Chem. XXXX, XXX, XXX−XXX

Nanoporous photonic crystals present a set of advantages over their solid counterparts: namely, (i) nanopores that can accommodate capturing molecules, increasing the specific surface area for sensing, (ii) nanopores that can act as physical filters to separate analytes, and (iii) ability to engineer the interaction light matter to enhance the sensing performance.[25,26] The pore geometry of NAA can be precisely engineered by different electrochemical approaches. Therefore, the effective medium of this nanoporous material can be rationally engineered in order to create a set of photonic crystal structures such as distributed Bragg reflectors, optical microcavities, waveguides, Fabry–Pérot interferometers, and rugate filters, which are the base of a broad range of optical sensing systems.[27−39] Among these photonic crystal structures, rugate filters (RFs) are of special interest given that their optical spectrum features a well-resolved intense characteristic reflection peak. When the effective medium of a NAA-RF is modified, its characteristic reflection peak undergoes shifts that can be used as sensing principle to detect analytes of interest or establish kinetic parameters associated with biological binding events. Recently, we reported on an innovative anodization approach, so-called sinusoidal pulse anodization, aimed at producing NAA-RFs with finely tuned photonic properties.[40]

Herein, we assess and establish the binding affinity between a set of drugs and HSA by combining HSA-modified NAA-RFs with RIfS. First, the nanoporous structure of NAA-RFs is systematically optimized by evaluating the binding affinity between HSA-modified NAA-RFs and indomethacin, a model drug. NAA-RFs are optimized following a design of experiments (DoE) approach as a function of two fabrication parameters (i.e., anodization period and anodization offset) focusing on maximizing the sensitivity on the sensor performance. Finally, the most sensitive HSA-modified NAA-RF structures are used as optical platforms combined with RIfS to establish the binding affinity between HSA as proof of the versatility of this system to be used as a generic device for establishing protein binding affinity.

EXPERIMENTAL SECTION

Materials. High-purity (99.9997%) 1.5 × 1.5 cm^2 square aluminum (Al) substrates 0.32 mm thick were supplied by Goodfellow Cambridge Ltd. (UK). Sulfuric acid (H_2SO_4), phosphoric acid (H_3PO_4), perchloric acid ($HClO_4$), hydrochloric acid (HCl), copper(II) chloride ($CuCl_2$), (3-aminopropyl)triethoxysilane (APTES), hydrogen peroxide (H_2O_2), glutaraldehyde (GTA, $C_5H_8O_2$), human serum albumin (HSA), phosphate buffered saline (PBS), indomethacin ($C_{19}H_{16}ClNO_4$), coumarin ($C_9H_6O_2$), sulfadymethoxine ($C_{12}H_{14}N_4O_4S$), warfarin ($C_{19}H_{16}O_4$), salicylic acid ($C_7H_6O_3$), and ethanol (EtOH, C_2H_5OH) were purchased from Sigma-Aldrich (Australia) and used as received, without further purification. All the aqueous solutions used in this study were prepared using ultrapure water Option Q-Purelabs (Australia).

Fabrication of Nanoporous Anodic Alumina Rugate Filters. NAA-RFs were fabricated following a sinusoidal pulse anodization approach under mild conditions and galvanostatic mode (i.e., current density control) in sulfuric acid electrolyte.[40] A definition of the different parameters of the sinusoidal anodization waves used in our study and a representative anodization profile used to produce NAA-RFs photonic crystal structure are shown in Figure 1a. Prior to anodization, Al substrates were cleaned under sonication in ethanol (EtOH) and distilled water for 15 min each and finally dried under air stream. Subsequently, Al substrates were electropolished using a mixture of $HClO_4$ and EtOH 1:4 (v:v) at 20 V and 5 °C for 3 min. After electropolishing, Al substrates were anodized in a thermally isolated custom-built anodization reactor using an aqueous solution 1.1 M sulfuric acid, the temperature of which was kept at −1 °C throughout the whole process. The anodization process started with a first stage at constant current density of 1.12 mA cm^{-2} for 1 h. Then, the sinusoidal pulse mode was set in order to engineer the effective medium of NAA in depth (Figure 1b). During this process, the anodization current density was modified in a sinusoidal fashion between high (J_{Max} = 1.12 mA cm^{-2}) and low (J_{Min} = J_{Offset} = 0.28 mA cm^{-2}) values according to eq 1:

$$J(t) = A_J \cdot \left[\sin\left(\frac{2\pi}{T_P} \cdot t \right) + 1 \right] + J_{Offset} \quad (1)$$

Here $J(t)$ is the current density at a given time t, A_J is the current density amplitude, T_P is the anodization period, and J_{Offset} is the current density offset (see Figure 1a).

It is worth noting that the nanoporous layer created during the first stage of this process was used as a shuttle to achieve a homogeneous pore growth before setting anodization to sinusoidal mode. Furthermore, the electrolyte solution was modified with 25 v% of EtOH in order to prevent it from freezing at temperatures below 0 °C.[41,42] Finally, the pore size of NAA-RFs was widened by wet chemical etching in an aqueous solution 5 wt % H_3PO_4 at 35 °C for 6 min. This enlargement of the pore size made possible the flow of HSA molecules inside the nanopores of NAA-RFs in order to create the desired surface chemistry for drug binding affinity assessment. Note that these photonic crystals were coated with a thin film of gold of 5 nm using a sputter coater equipped with film thickness monitor (sputter coater 108auto, Cressington) in order to enhance the interference effect and enhance the RIfS signal for sensing experiments.[43,44] Furthermore, the underlying aluminum substrate was chemically removed in a saturated solution of $HCl/CuCl_2$ using an etching cell with a window of 8 mm in diameter.

Optical Characterization. Shifts in the characteristic reflection peak position ($\Delta\lambda_{Peak}$) and changes in the effective optical thickness (ΔOT_{eff}) of HSA-modified NAA-RFs produced as a result of the binding with drug molecules were monitored by a RIfS system composed of a bifurcated optical probe that focuses white light from a light source (LS-1LL, Ocean Optics) on the surface of NAA-RFs. The illumination spot was adjusted to 2 mm in diameter by a lens system (VIS Collimating Lens, 350−2000 nm, Ocean Optics). The reflected light was collected by the collection fiber, which is assembled around the same optical probe, and directly transferred to a miniature spectrometer (USB4000+VIS-NIR-ES, Ocean Optics). The reflection spectra of NAA-RFs were acquired from 400 to 1000 nm and saved at intervals of 30 s, with an integration time of 10 ms and 10 average measurements. RIfS spectra were processed in Igor Pro library (Wavemetrics) in order to estimate $\Delta\lambda_{Peak}$ and ΔOT_{eff}.

Optimization of HSA-Modified NAA-RFs. Two anodization parameters (i.e., anodization period T_P and anodization offset J_{Offset} − k = 2) were systematically modified in order to establish the optimization path between the fabrication parameters and the sensitivity of the NAA-RFs-RIfS system. T_P and J_{Offset} were modified from 650 to 750 s (ΔT_P = 50 s) and from 0.140 to 0.420 mA cm^{-2} with ΔJ_{Offset} = 0.105 mA

DOI: 10.1021/acs.analchem.6b00993
Anal. Chem. XXXX, XXX, XXX−XXX

cm^{-2}, respectively. The rest of the anodization parameters were kept constant in all these samples [i.e., A_J = 0.42 mA cm^{-2} and number of sinusoidal pulses (N_P) = 150 pulses]. Therefore, a set of nine NAA-RFs (3^2 = 9) were fabricated following the aforementioned approach (Table 1). These NAA-RFs were chemically functionalized in order to determine the most sensitive HSA-modified NAA-RF structure toward indomethacin molecules as a function of T_P and J_{Offset}. In this process, NAA-RFs were first silanized with APTES following a well-established functionalization process.[45,46] Briefly, NAA-RFs were hydroxylated in H_2O_2 30 wt % for 10 min at 90 °C in order to increase the number of hydroxyl groups on the surface of alumina. Subsequently, hydroxylated NAA-RFs were modified with APTES by chemical vapor deposition process under vacuum at 110 °C for 3 h. After APTES modification, NAA-RFs were washed with ethanol and water, dried under an air stream, and stored under dry conditions until further use. Both the immobilization of HSA and the detection of indomethacin molecules were performed in real-time by RIfS using an acrylic-based flow cell. Shifts in the characteristic reflection peak position of each NAA-RF (λ_{Peak}) and changes in the effective optical thickness of the whole film (OT_{eff}) were monitored in real-time by RIfS. Five analytical solutions of indomethacin (1, 2, 3, 4, and 5 mM) were prepared in PBS modified with 5 v% EtOH in order to increase the solubility of this hydrophobic drug. Note that the different solutions were flowed through the flow cell at a constant rate of 100 μL min^{-1} by a syringe pump (Fusion 200 Touch series, Chemyx Inc.). Table 1 provides a comprehensive summary of these NAA-RFs (experimental matrix), the objective of which was to evaluate

Table 1. Summary of the Fabrication Conditions Used To Produce the Nanoporous Anodic Alumina Rugate Filters Utilized in This Study To Establish the Binding Affinity between Drugs and Human Serum Albumin Molecules

	J_{Offset} (mA cm^{-2})		
T_P (s)	0.14	0.28	0.42
650	NAA-$RF_{650-0.14}$	NAA-$RF_{650-0.28}$	NAA-$RF_{650-0.42}$
700	NAA-$RF_{700-0.14}$	NAA-$RF_{700-0.28}$	NAA-$RF_{700-0.42}$
750	NAA-$RF_{750-0.14}$	NAA-$RF_{750-0.28}$	NAA-$RF_{750-0.42}$

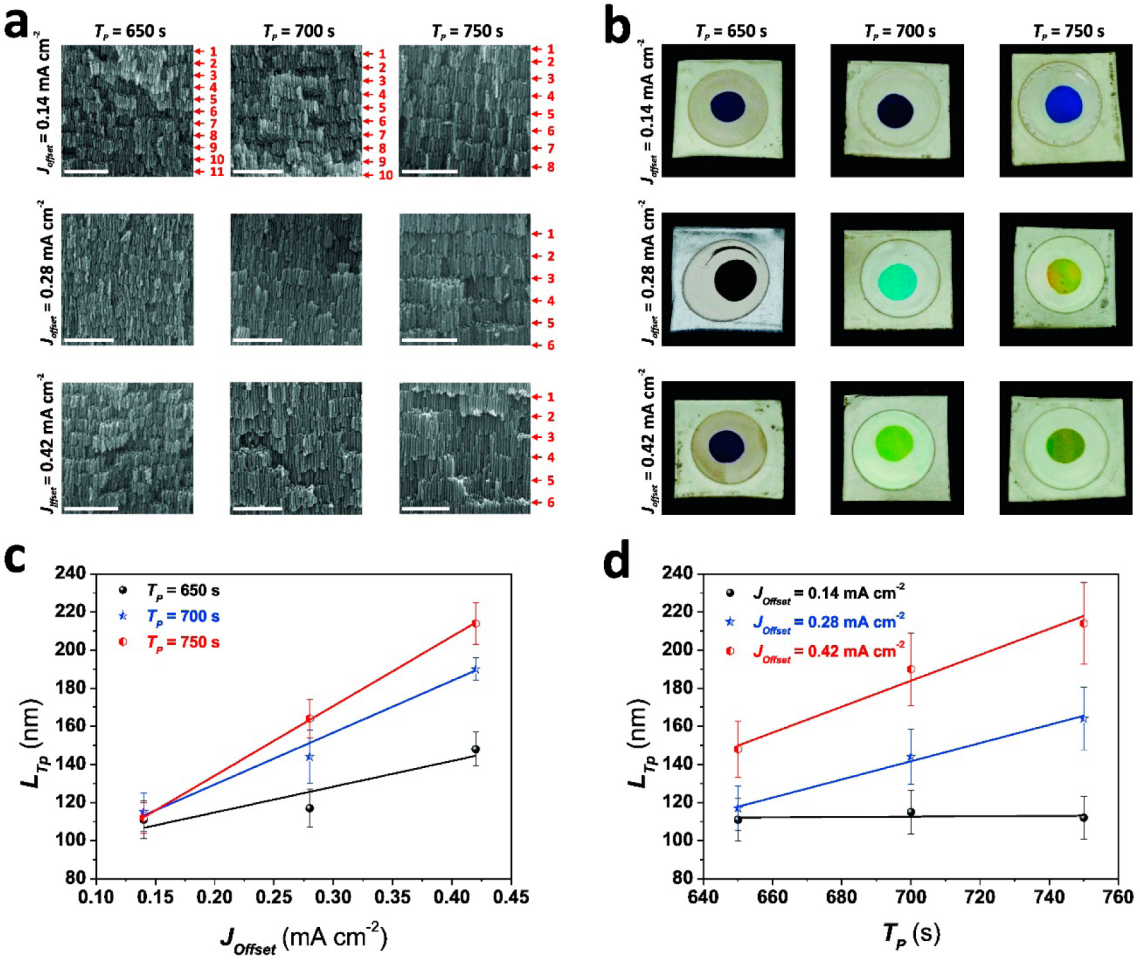

Figure 2. Tunability of the characteristic period length (L_{Tp}) in NAA-RFs by the anodization period (T_P) and the anodization offset (J_{Offset}). (a) Magnified cross-section view SEM images of NAA-RFs produced with T_P = 650, 700, and 750 s and J_{Offset} = 0.14, 0.28, and 0.42 mA cm^{-2} (fixed parameters: A_J = 0.42 mA cm^{-2}, N_P = 150 pulses, T_{An} = −1 °C, and t_{pw} = 6 min) (scale bars = 500 nm) (note that red arrows in these images denote the interfaces between consecutive anodization periods, L_{Tp}). (b) Digital pictures of these NAA-RFs displaying different interferometric colors as a function of T_P and J_{Offset} (note that the underlying aluminum substrate was chemically etched away in a saturated solution of $HCl/CuCl_2$ using an etching cell with a window of 8 mm in diameter). (c) Linear dependence of L_{Tp} on J_{Offset} for T_P = 650, 700, and 750 s. (d) Linear dependence of L_{Tp} on T_P for J_{Offset} = 0.14, 0.28, and 0.42 mA cm^{-2}.

DOI: 10.1021/acs.analchem.6b00993
Anal. Chem. XXXX, XXX, XXX−XXX

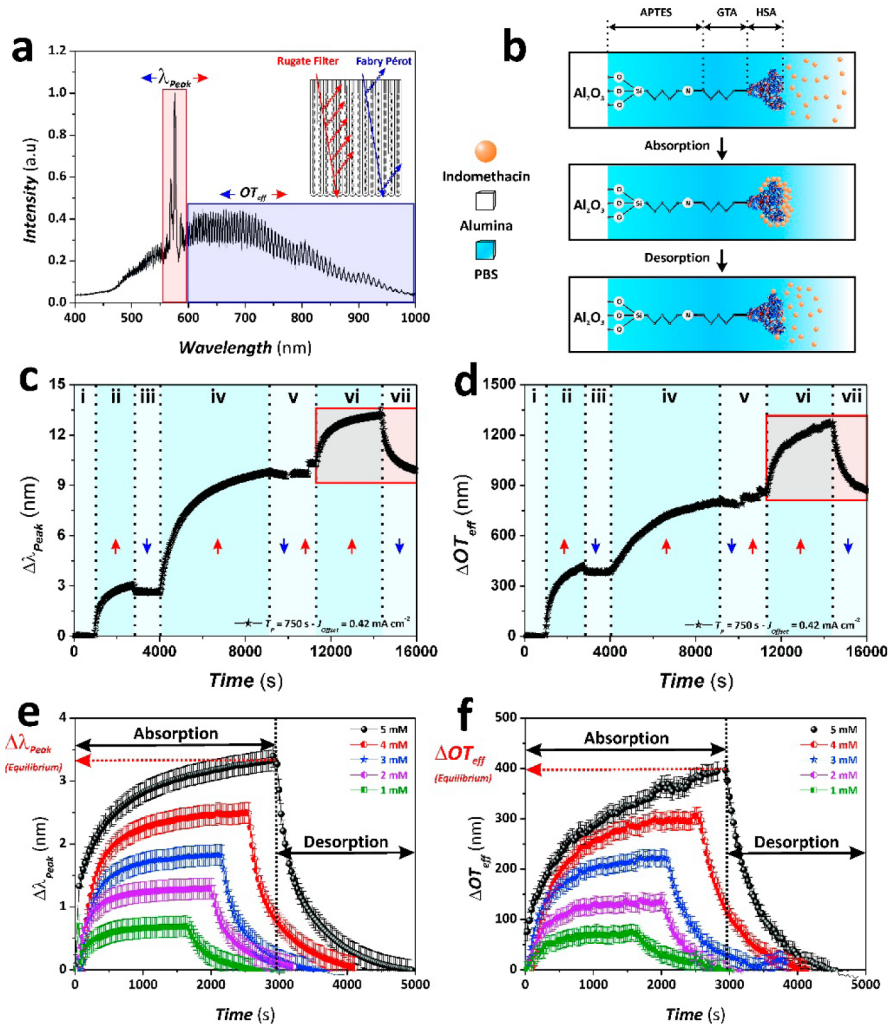

Figure 3. Sensing concept used to establish the binding affinity between HSA and indomethacin molecules by combining HSA-functionalized NAA-RFs and RIfS. (a) Representative RIfS spectrum of a NAA-RF (T_P = 650 s, J_{Offset} = 0.42 mA cm^{-2}, and t_{pw} = 0 min) showing the areas in the spectrum used to establish changes in λ_{Peak} and OT_{eff} associated with binding between HSA and indomethacin molecules. (b) Schematic illustration describing the reversible binding event between HSA and indomethacin molecules with adsorption and desorption stages after injection of indomethacin analytical solutions and fresh PBS, respectively. (c, d) Representative real-time measurements for $\Delta\lambda_{Peak}$ and ΔOT_{eff} showing the shifts in the position of the characteristic peak position and changes in the effective optical thickness of NAA-RFs during the different stages (blue and red arrows indicate areas where $\Delta\lambda_{Peak}$ and ΔOT_{eff} undergo blue and red shifts, respectively): (i) PBS baseline, (ii) GTA activation, (iii) PBS washing, (iv) HSA immobilization, (v) PBS washing and PBS−EtOH baseline, (vi) indomethacin detection in PBS−EtOH, and (vii) PBS−EtOH washing (note the example corresponding to a NAA-RF produced with T_P = 750 s and J_{Offset} = 0.42 mA cm^{-2}). (d) Detail of the absorption and desorption stages (red square in parts c and d) for $\Delta\lambda_{Peak}$ and ΔOT_{eff} vs time as a function of the concentration of indomethacin (1, 2, 3, 4, and 5 mM).

the effect of each of these parameters on the photonic properties and sensitivity (S) of NAA-RFs measured by two parameters: namely, (i) changes in the position of the characteristic reflection peak ($\Delta\lambda_{Peak}$) and (ii) changes in the effective optical thickness of the whole NAA-RF (ΔOT_{eff}). We applied an analysis of variance (ANOVA) for a 3^k-factorial design of experiments (DoE) in order to discern objectively the effect of T_P and J_{Offset} on the studied variable (i.e., S, sensitivity of HSA-modified NAA-RFs toward indomethacin molecules).[47,48] A DoE strategy makes it possible to optimize the number of experiments while establishing possible quadratic effects in the relationship between the anodization parameters and the sensitivity of the NAA-RFs-RIfS system.

In this study, three null hypotheses were tested by means of the aforementioned ANOVA test, namely, the following, if α_i and β_j quantify the effects of T_P and J_{Offset}, respectively.:

(i) H_0, $\alpha_i = 0$ (there is no significant effect of T_P on S);

(ii) H_1, $\beta_j = 0$ (there is no significant effect of J_{Offset} on S);

(iii) H_2, $(\alpha\cdot\beta)_{ij} = 0$ (there is no significant effect of the anodization parameters interaction (i.e., $T_P\cdot J_{Offset}$) on S).

If these hypotheses were rejected, the alternative hypotheses would be accepted. These alternative hypotheses are the following:

(i*) H_0*, $\alpha_i \neq 0$ (there is a significant effect of T_P on S);

(ii*) H_1*, $\beta_j \neq 0$ (there is a significant effect of J_{Offset} on S);

(iii*) H_2*, $(\alpha\cdot\beta)_{ij} \neq 0$ (there is a significant effect of the anodization parameters interaction (i.e., $T_P\cdot J_{Offset}$) on S).

Establishment of Binding Affinity between Drugs and HSA-Modified NAA-RFs by RIfS. A set of the most sensitive NAA-RF structures for each of the aforementioned sensing parameters (i.e., $\Delta\lambda_{Peak}$ and ΔOT_{eff}) toward indomethacin molecules were fabricated and functionalized following the above-mentioned anodization and silanization protocols. These

DOI: 10.1021/acs.analchem.6b00993
Anal. Chem. XXXX, XXX, XXX−XXX

samples were used to assess the binding affinity between HSA molecules immobilized onto NAA-RFs and a set of drug model molecules, including indomethacin, coumarin, sulfadymethoxine, warfarin, and salicylic acid. These sensing experiments were performed according to the process shown in the Optical Characterization section using $\Delta\lambda_{Peak}$ and ΔOT_{eff} as sensing parameters (*vide supra*).

Structural Characterization. The structural characteristics of NAA-RFs were established by a field emission gun scanning electron microscope (FEG-SEM FEI Quanta 450). These images were subsequently analyzed by ImageJ (public domain program developed at the RSB of the NIH) in order to measure the period length in the different NAA-RF structures.[49]

All the aforementioned experiments were repeated three times with freshly modified NAA-RFs and analytical solutions, and the characteristic parameters were calculated as averages and standard deviations.

RESULTS AND DISCUSSION

Structural Characterization and Optical Optimization of NAA-RFs. The optical properties and sensing performance of NAA-RFs are strongly dependent on the period thickness (L_{Tp}) (Figure 1b). Figure 1c shows representative cross-section and top view images of NAA-RFs. These photonic structures are composed of stacked layers of nanopores with sinusoidally modified porosity in depth, which are generated by the sinusoidal fabrication process described above. Figure 2a shows cross-section SEM images with magnified views of the NAA-RFs used in this study, which were produced using nine different combinations of T_P and J_{Offset} (see Table 1). Digital images of these photonic films reveal that the interferometric color, an optical property established by the position of the characteristic reflection peak (λ_{Peak}), undergoes a red shift toward longer wavelengths when T_P and J_{Offset} increase (Figure 2b).[40] SEM image analysis reveals that L_{Tp} increases linearly with the anodization period and the anodization offset (Figure 2c,d). Nevertheless, we found slight differences in the dependence of L_{Tp} with T_P and J_{Offset}. As Figure 2c shows, the longer the anodization period is, the stronger the dependence is for L_{Tp} on J_{Offset}. The slope of the fitting line for the dependence of L_{Tp} on J_{Offset} for T_P = 650, 700, and 750 s was found to be 135 ± 50, 272 ± 23, and 365 ± 4 nm (mA cm^{-2})$^{-1}$, respectively. Figure 2d shows the linear fittings describing how L_{Tp} varies with T_P for the different values of J_{Offset}. This graph reveals that the dependence of L_{Tp} on T_P for J_{Offset} = 0.14, 0.28, and 0.42 mA cm^{-2} was 0.0162 ± 0.04, 0.477 ± 0.04, and 0.680 ± 0.10 nm s^{-1}, respectively.

Optimization of Sensing Performance of HSA-Modified NAA-RFs Combined with RIfS. The above-mentioned NAA-RFs (Table 1) were modified with human serum albumin and used as sensing platforms to establish the binding affinity between immobilized HSA and indomethacin molecules as a function of the fabrication parameters (i.e., T_P and J_{Offset}). Indomethacin is commonly used as a prescription drug to reduce stiffness, fever, pain, and swelling. This drug was used as a model drug molecule due to its well-known affinity toward HSA and other serum proteins. In this study, two sensing parameters were used in order to establish the most sensitive NAA-RF structures toward indomethacin molecules: namely, (i) shifts in the characteristic reflection peak ($\Delta\lambda_{Peak}$) and (ii) changes in the effective optical thickness of the film (ΔOT_{eff}). Whereas the former parameter was established by following the position of λ_{Peak} in the RIfS spectrum of NAA-RFs, the latter was obtained by applying fast Fourier transform to the RIfS spectrum of NAA-RFs.[50] Figure 3a (inset) shows a schematic illustration of a NAA rugate filter and the interfering light beams at the different interfaces forming these photonic crystal structures. The reflectivity spectrum of NAA-RFs is derived from two sources: namely, (i) the interference of light from all layers of the multilayered NAA-RF structure and (ii) the Fabry−Pérot interference spectrum produced by the reflections of light at the interfaces bordering the NAA-RF film.[50] As a result, the RIfS spectrum of NAA-RFs displays a narrow and well-defined characteristic reflection peak, which corresponds to the photonic stop band of the photonic crystals, and small sideband fringes produced by the Fabry−Pérot interference in the photonic film (Figure 3a). In our experiments, the characteristic reflection peak (λ_{Peak}) was separated from the Fabry−Pérot fringes region in order to apply an FFT to the selected region and estimate the effective optical thickness (OT_{eff}) of the film.[50] Both optical parameters were used as sensing references to establish the most sensitive NAA-RFs structures toward indomethacin molecules. Figure 3b shows a schematic illustration of the sensing approach used in our study to establish the binding affinity between drug molecules and HSA-modified NAA-RFs. Figure 3c,d displays examples of this process using HSA-modified NAA-RFs and RIfS with $\Delta\lambda_{Peak}$ and ΔOT_{eff} as the sensing reference parameters, respectively. This process is divided into three stages: (i) chemical activation of amine ($-NH_2$) groups present on the surface of NAA by GTA, (ii) immobilization of HSA molecules on the surface of activated NAA-RFs, and (iii) adsorption−desorption of drug molecules from HSA-modified NAA-RFs. First, fresh PBS (pH 7.4) solution was flowed at a rate of 100 μL min^{-1} through the flow cell, where APTES-functionalized NAA rugate filters were placed. A stable baseline for $\Delta\lambda_{Peak}$ and ΔOT_{eff} was achieved after 15 min (i, Figure 3c,d). After this, a 2.5 v% GTA solution in PBS was flowed through the system for 30 min in order to activate the amine groups present on the inner surface of NAA-RFs (ii, Figure 3c,d). In this stage, $\Delta\lambda_{Peak}$ and ΔOT_{eff} underwent a red shift due to the interaction between activated amine groups present on the inner surface of NAA-RFs and GTA molecules. Fresh PBS solution was flowed again after GTA activation for 15 min in order to remove physisorbed GTA molecules from the surface of NAA-RFs. As a result, $\Delta\lambda_{Peak}$ and ΔOT_{eff} decreased slightly during this process (iii, Figure 3c,d). Next, a 1 mg mL^{-1} solution of HSA in PBS was injected into the system and flowed at 100 mL min^{-1} for 1 h (iv, Figure 3c,d). A marked red shift was observed both in sensing parameters as a result of the binding event between GTA-activated APTES-modified NAA-RFs and HSA molecules.

Then, fresh PBS solution was flowed through the flow cell in order to wash away physisorbed HSA molecules (v, Figure 3c,d). Prior to injection of indomethacin analytical solutions, a baseline in a modified PBS solution containing EtOH 5 v% was obtained for 15 min in order to compensate the addition of ethanol to improve the solubility of indomethacin, which is a highly hydrophobic therapeutic. The binding interaction between HSA and indomethacin molecules present in the PBS solution resulted in a sharp red shift both in $\Delta\lambda_{Peak}$ and ΔOT_{eff} (vi, Figure 3c,d), which continued until the HSA molecules present in the inner surface of NAA-RFs were saturated by indomethacin molecules (i.e., equilibrium stage = end of vi, Figure 3c,d). After this, fresh PBS solution containing 5 v% EtOH was flowed through the system in order to desorb

DOI: 10.1021/acs.analchem.6b00993
Anal. Chem. XXXX, XXX, XXX−XXX

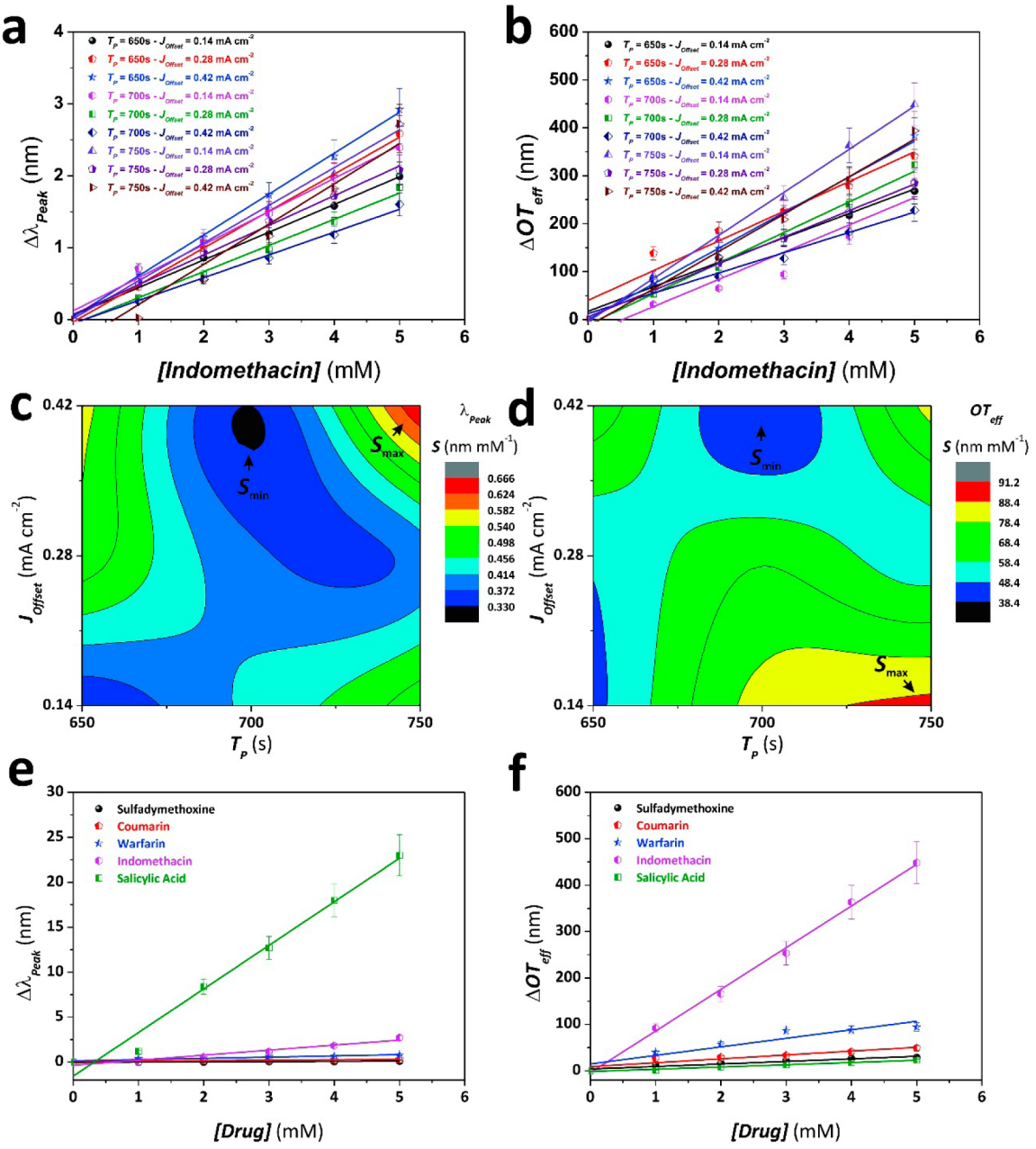

Figure 4. Optical optimization and establishment of binding affinity between drug molecules and HSA-modified NAA-RFs by RIfS. (a) Linear fitting lines showing the linear dependence between $\Delta\lambda_{Peak}$ and the different concentrations of indomethacin (1, 2, 3, 4, and 5 mM) for each type of NAA-RF. (b) Linear fitting lines showing the linear dependence between ΔOT_{eff} and the different concentrations of indomethacin (1, 2, 3, 4, and 5 mM) for each type of NAA-RF. (c) Contour map showing the distribution of sensitivity (S) as a function of the fabrication parameters (i.e., T_P and J_{Offset}) for $\Delta\lambda_{Peak}$ calculated from part a. (d) Contour map showing the distribution of sensitivity (S) as a function of the fabrication parameters (i.e., T_P and J_{Offset}) for ΔOT_{eff} calculated from part b. (e) Linear fitting lines showing the dependence between $\Delta\lambda_{Peak}$ and the different concentrations of the drugs assessed in this study for NAA-$RF_{750-0.42}$. (f) Linear fitting lines showing the dependence between ΔOT_{eff} and the different concentrations of the drugs assessed in this study for NAA-$RF_{750-0.14}$.

indomethacin from HSA molecules (vii, Figure 3c,d). Note that the binding event between indomethacin molecules and HSA molecules is a reversible reaction. Therefore, both $\Delta\lambda_{Peak}$ and ΔOT_{eff} underwent a blue shift until the original baseline (i.e., vi, Figure 3c,d) was reached. A summary of the obtained results for $\Delta\lambda_{Peak}$ and ΔOT_{eff} for each analytical solution of indomethacin (1, 2, 3, 4, and 5 mM) are displayed in Figure 3e,f. This process is characterized by two stages: (i) adsorption stage, when the analytical solution of drug is injected into the flow cell, and (ii) desorption stage, when fresh PBS solution is flowed through the flow cell and drug molecules are released from HSA. The total changes in $\Delta\lambda_{Peak}$ and ΔOT_{eff} can be calculated as indicated in Figure 3e,f.

Figure 4a,b shows the linear fittings for $\Delta\lambda_{Peak}$ and ΔOT_{eff} as a function of the concentration of indomethacin for the different NAA-RFs structures used in this study (Table 1). These graphs show that $\Delta\lambda_{Peak}$ and ΔOT_{eff} have a linear dependence with the concentration of indomethacin. A linear fitting between $\Delta\lambda_{Peak}$ and ΔOT_{eff} and the concentration of indomethacin makes it possible to estimate the sensitivity, S

DOI: 10.1021/acs.analchem.6b00993
Anal. Chem. XXXX, XXX, XXX−XXX

(i.e., slope of the fitting line), the low limit of detection, LLoD (i.e., calculated as 3σ), and the linearity, R^2 (i.e., correlation coefficient of the fitting line), for each NAA-RF. The obtained results, summarized in Table S1 (Supporting Information), reveal that the NAA-RF structures with the highest sensitivity for $\Delta\lambda_{Peak}$ and ΔOT_{eff} were NAA-$RF_{750-0.42}$ (S = 0.66 ± 0.03 nm mM^{-1}, LLoD = 0.65 ± 0.02 mM, and R^2 = 0.985) and NAA-$RF_{750-0.14}$ (S = 91.1 ± 3.4 nm mM^{-1}, LLoD = 0.41 ± 0.03 mM, and R^2 = 0.994), respectively. Figure 4c,d shows contour maps displaying the dependence of S on the fabrication parameters (T_P and J_{Offset}) for $\Delta\lambda_{Peak}$ and ΔOT_{eff}. These graphs denote that the distribution of S with T_P and J_{Offset} is fairly homogeneous for both the cases (i.e., $\Delta\lambda_{Peak}$ and ΔOT_{eff}) since the distribution of color fields (i.e., increment in S) is concentrically homogeneous around the minimum values, which are located at T_P = 700 s and J_{Offset} = 0.14 mA cm^{-2} for $\Delta\lambda_{Peak}$ and ΔOT_{eff}. However, although the lines between color fields are closer to each other in a similar manner, it is worth noting that contour lines in $\Delta\lambda_{Peak}$ are much closer around the proximity of the maximum value (T_P = 750 s and J_{Offset} = 0.42 mA cm^{-2}) than those of ΔOT_{eff}, indicating a much stronger dependence of S on T_P and J_{Offset}. In order to gain a more objective insight into the dependence of S on T_P and J_{Offset}, we performed an ANOVA analysis for the sensitivity obtained by measuring both sensing parameters ($\Delta\lambda_{Peak}$ and ΔOT_{eff}).

The ANOVA analysis (Table 2) was performed using the values of S measured from $\Delta\lambda_{Peak}$ and ΔOT_{eff}, and the values of each parameter were estimated using the equations shown in Table S2 (Supporting Information). In this analysis, the hypotheses H_0, H_1, and H_2 are assessed by comparing the value of F_0 (i.e., test statistic calculated from the ANOVA table) and the corresponding value of the F-distribution for a significance level of 95%. Our analysis for S obtained from $\Delta\lambda_{Peak}$ denotes that the hypotheses H_0 and H_1 are both rejected since the individual effects of these anodization parameters are significant (i.e., 166.9 and 66.9 > $F_{(0.05;2;27)}$ = 3.4, respectively). Therefore, the alternative hypotheses H_0* and H_1* are accepted. This analysis also reveals that the interaction between T_P and J_{Offset} (T_P·J_{Offset}) is significant as well because 119.0 > $F_{(0.05;4;27)}$ = 2.7. Thus, the hypothesis H_2 is also rejected and the alternative hypothesis H_2* accepted. As a result, it is concluded that all the fabrication parameters (i.e., T_P, J_{Offset}, and their interaction T_P·J_{Offset}) have a significant effect over S. Nevertheless, the magnitudes of H_0*, H_1*, and H_2* have different weight over the studied variable S, being 47.3%, 19.0%, and 33.7% for T_P, J_{Offset}, and their interaction T_P·J_{Offset}, respectively. Hence, S is found to have a stronger dependence on T_P when $\Delta\lambda_{Peak}$ is used as the sensing parameter.

As far as the ANOVA analysis on S obtained from ΔOT_{eff} is concerned, it shows that the hypotheses H_0 and H_1 are both rejected as the individual effects of T_P and J_{Offset} are both significant (i.e., 51.7 and 36.6 > $F_{(0.05;2;27)}$ = 3.4, respectively). As a result, the alternative hypotheses H_0* and H_1* are accepted. Furthermore, it is found that the interaction between T_P and J_{Offset} (T_P·J_{Offset}) is also significant since 84.8 > $F_{(0.05;4;27)}$ = 2.7. Therefore, the hypothesis H_2 is rejected and the alternative hypothesis H_2* accepted. In this case, it is established that T_P, J_{Offset}, and their interaction T_P·J_{Offset} all have a significant effect over S. However, the magnitudes of H_0*, H_1*, and H_2* have weights of 29.9%, 21.1%, and 49.0%. Therefore, S has a more marked dependence on the interaction T_P·J_{Offset} when ΔOT_{eff} is used as the sensing parameter.

Table 2. Summary of the ANOVA Analysis Performed in Our Study To Establish the Most Optimal NAA-RF Structures As a Function of the Fabrication Parameters (T_P and J_{Offset})

source of variance	SS	DF	MS	F_0
Sensing Parameter $\Delta\lambda_{Peak}$				
T_P (s)	0.1032	2	0.0516	166.9
J_{Offset} (mA cm^{-2})	0.0414	2	0.0207	66.9
T_P·J_{Offset} (s mA cm^{-2})	0.1472	4	0.0368	119.0
model	0.2917	8	0.0365	117.9
error	0.0056	18	3.0922	
total	0.2973	26		
Sensing Parameter ΔOT_{eff}				
T_P (s)	1688.9	2	844.4	51.7
J_{Offset} (mA cm^{-2})	1195.1	2	597.6	36.6
T_P·J_{Offset} (s mA cm^{-2})	5545.6	4	1386.4	84.8
model	8429.6	8	1053.7	64.5
error	294.2	18	16.3	
total	8723.9	26		

Assessment of Binding Affinity between Drugs and HSA-Modified NAA-RFs by RIfS. A set of the most sensitive NAA-RFs structures toward indomethacin molecules (NAA-$RF_{750-0.42}$ and NAA-$RF_{750-0.14}$ for $\Delta\lambda_{Peak}$ and ΔOT_{eff}, respectively) were used in order to establish the binding affinity between a set of drugs (i.e., indomethacin, coumarin, sulfadymethoxine, warfarin, and salicylic acid) and HSA molecules by RIfS using $\Delta\lambda_{Peak}$ and ΔOT_{eff} as sensing parameters. This set of experiments was carried out following the above-mentioned protocol (*vide supra*) in a flow cell where five analytical solutions of each drug (1, 2, 3, 4, and 5 mM) were flowed at a constant rate (100 μL min^{-1}). The obtained results for $\Delta\lambda_{Peak}$ and ΔOT_{eff} are summarized in Table 3 and Figure 4e,f, respectively. $\Delta\lambda_{Peak}$ establishes that the binding

Table 3. Summary of Binding Affinity between Drug Molecules and HSA-Functionalized NAA-RFs Obtained from $\Delta\lambda_{Peak}$ (NAA-$RF_{750-0.42}$) and ΔOT_{eff} (NAA-$RF_{750-0.14}$) and Comparison with the Binding Affinity Reported in the Literature

	sensing parameter				
	$\Delta\lambda_{Peak}$		ΔOT_{eff}		
drug	S (nm mM^{-1})	level	S (nm mM^{-1})	level	literature[a] level
indomethacin	0.560 ± 0.067	M	89.8 ± 2.3	H	H
sulfadymethoxine	0.027 ± 0.005	L	5.5 ± 0.7	M	H
warfarin	0.138 ± 0.024	M	18.4 ± 3.2	H	H
coumarin	0.045 ± 0.012	L	8.3 ± 1.7	M	M
salicylic acid	4.850 ± 0.317	H	4.9 ± 0.3	M	M

[a]Values obtained from ref 9.

DOI: 10.1021/acs.analchem.6b00993
Anal. Chem. XXXX, XXX, XXX−XXX

affinity between HSA and the aforementioned set of drugs follows the order salicylic acid (S = 4.850 ± 0.317 nm mM^{-1}) > indomethacin (S = 0.560 ± 0.067 nm mM^{-1}) > warfarin (S = 0.138 ± 0.024 nm mM^{-1}) > coumarin (S = 0.045 ± 0.012 nm mM^{-1}) > sulfadymethoxine (S = 0.027 ± 0.005 nm mM^{-1}). In contrast, ΔOT_{eff} establishes that the binding affinity between these drugs and HSA molecules follows the order indomethacin (S = 89.8 ± 2.3 nm mM^{-1}) > warfarin (S = 18.4 ± 3.2 nm mM^{-1}) > coumarin (S = 8.3 ± 1.7 nm mM^{-1}) > sulfadymethoxine (S = 5.5 ± 0.7 nm mM^{-1}) > salicylic acid (S = 4.9 ± 0.3 nm mM^{-1}).

Previous studies have reported that, whereas the binding affinity between indomethacin, sulfadymethoxine, warfarin, and HSA molecules is high, coumarin and salicylic acid present an interaction with medium strength toward this plasma protein.[9] Our results using $\Delta\lambda_{Peak}$ as the sensing parameter establish salicylic acid as a drug molecule with high affinity toward HSA molecules, whereas indomethacin and warfarin have medium affinity, and coumarin and sulfadymethoxine present a low affinity toward HSA. However, indomethacin and warfarin have high affinity toward HSA molecules, and coumarin, sulfadymethoxine, and salicylic acid are found to be drug molecules with medium affinity when ΔOT_{eff} is used as the sensing parameter. These results reveal a higher degree of agreement between the results obtained by benchmark techniques[9] and those obtained in this study by ΔOT_{eff}. Therefore, it can be concluded that ΔOT_{eff} is a more reliable sensing parameter than $\Delta\lambda_{Peak}$ to be used in the proposed sensing system combining NAA-RFs and RIfS.

CONCLUSIONS

This study has reported on an approach that aims to assess the binding affinity between drug molecules and human serum albumin by combining HSA-modified NAA-RFs with RIfS. First, we carried out a systematic analysis of the structural features and optical properties of NAA-RFs produced by sinusoidal pulse anodization. These photonic crystal structures present two characteristic optical parameters, the characteristic reflection peak (λ_{Peak}), and the effective optical thickness of the film (OT_{eff}), which can be readily used as sensing parameters. A set of nine NAA-RFs were used to establish the most sensitive structures toward indomethacin molecules, a model drug, as a function of two fabrication parameters (i.e., T_P, anodization period, and J_{Offset}, anodization offset). A design of experiment strategy made it possible to establish the effect of these anodization parameters on the sensitivity of HSA-modified NAA-RFs using two sensing parameters, that is, shifts in the characteristic reflection peak ($\Delta\lambda_{Peak}$) and changes in the effective optical thickness of the film (ΔOT_{eff}). An ANOVA analysis established that the anodization period, the anodization offset, and their interaction have all significant effects on the sensing performance of NAA-RFs for both sensing parameters (i.e., $\Delta\lambda_{Peak}$ and ΔOT_{eff}). Nevertheless, whereas T_P was found to be the parameter with the most significant influence over S in the case of $\Delta\lambda_{Peak}$, the interaction $T_P \cdot J_{Offset}$ was the parameter with the strongest influence over the sensitivity of NAA-RFs for ΔOT_{eff}. Our analysis also revealed that the most sensitive structures toward indomethacin molecules were NAA-$RF_{750-0.42}$ and NAA-$RF_{750-0.14}$ for $\Delta\lambda_{Peak}$ and ΔOT_{eff}, respectively. Subsequently, we used these NAA-RF structures in order to establish the binding affinity between a set of drugs (i.e., indomethacin, coumarin, sulfadymethoxine, warfarin, salicylic acid) and HSA molecules. We found that, in the case of NAA-RFs, the binding affinity between drug molecules and HSA is dependent on the sensing parameter used. Whereas $\Delta\lambda_{Peak}$ established salicylic acid as the drug molecule with the highest affinity toward HSA molecules, indomethacin was found to be the drug with the strongest affinity when ΔOT_{eff} was used as the sensing parameter. Although the low limit of detection achieved by our system is slightly higher than that of benchmark techniques such as SPR, the obtained results are certainly promising, and there is still margin for improvement by further optimization strategies. The proposed sensing system combining HSA-modified NAA-RFs and RIfS provides a reliable means of assessing the binding affinity of drugs with a set of features such as portability, low cost, and easy operation that makes it a promising alternative to benchmark techniques such as SPR.

ASSOCIATED CONTENT

Supporting Information

The Supporting Information is available free of charge on the ACS Publications website at DOI: 10.1021/acs.analchem.6b00993.

Further information about the fitting lines and sensing parameters used to establish the most sensitive NAA-RF structures and equations of ANOVA (PDF)

AUTHOR INFORMATION

Corresponding Authors

*Phone: +61 8 8313 1535. Fax: +61 8 8303 4373. E-mail: abel.santos@adelaide.edu.au. Web page: http://www.adelaide.edu.au/directory/abel.santos.

*Phone: + 61 8 8313 4648. Fax: +61 8 8303 4373. E-mail: dusan.losic@adelaide.edu.au. Web page: http://www.adelaide.edu.au/directory/dusan.losic.

Author Contributions

A.S. conceived the idea and designed the experimental part of this work. N.M carried out the experiments assisted by C.S.L. and A.S. The obtained results were discussed and analyzed by all the authors. The final version of the manuscript was written through contributions of all the authors. All the authors have given approval to the final version of the manuscript.

Notes

The authors declare no competing financial interest.

ACKNOWLEDGMENTS

Authors acknowledge the support provided by the Australian Research Council (ARC) through Grants DE140100549, DP120101680, and FT110100711 and the School of Chemical Engineering (UoA). Authors thank the Adelaide Microscopy (AM) centre for FEG-SEM characterization.

ABBREVIATIONS

NAA-RF	nanoporous anodic alumina rugate filters
HSA	human serum albumin
RIfS	reflectometric interference spectroscopy

REFERENCES

(1) Munos, B. *Nat. Rev. Drug Discovery* **2009**, *8*, 959−968.
(2) Mullard, A. *Nat. Rev. Drug Discovery* **2011**, *10*, 82−85.
(3) Knutsen, L. J. S. *Drug Discovery Today* **2011**, *16*, 476−484.
(4) Khanna, I. *Drug Discovery Today* **2012**, *17*, 1088−1102.
(5) Kola, L.; Landis, J. *Nat. Rev. Drug Discovery* **2004**, *3*, 711−715.

DOI: 10.1021/acs.analchem.6b00993
Anal. Chem. XXXX, XXX, XXX−XXX

(6) Andersson, S.; Armstrong, A.; Björe, A.; Bowker, S.; Chapman, S.; Davies, R.; Donald, C.; Egner, B.; Elebring, T.; Holmqvist, S.; Inghardt, T.; Johannesson, P.; Johansson, M.; Johnstone, C.; Kemmitt, P.; Kihlberg, J.; Korsgren, P.; Lemurell, M.; Moore, J.; Pettersson, J. A.; Pointon, H.; Pontén, F.; Schofield, P.; Selmi, N.; Whittamore, P. *Drug Discovery Today* **2009**, *14*, 598−604.
(7) Oravcová, J.; Böhs, B.; Lindner, W. *J. Chromatogr., Biomed. Appl.* **1996**, *677*, 1−28.
(8) Hage, D.; Tweed, S. *J. Chromatogr., Biomed. Appl.* **1997**, *699*, 499−525.
(9) Frostell-Karlsson, A.; Remaeus, A.; Roos, H.; Andersson, K.; Borg, P.; Hämäläinen, M.; Karlsson, R. *J. Med. Chem.* **2000**, *43*, 1986−1992.
(10) Kraus, G.; Brecht, A.; Vasic, V.; Gauglitz, G. *Fresenius' J. Anal. Chem.* **1994**, *348*, 598−602.
(11) Yan, H. M.; Kraus, G.; Gauglitz, G. *Anal. Chim. Acta* **1995**, *312*, 1−8.
(12) Kraus, G.; Gauglitz, G. *Chemom. Intell. Lab. Syst.* **1995**, *30*, 211−221.
(13) Haake, H. M.; Schütz, A.; Gauglitz, G. *Fresenius' J. Anal. Chem.* **2000**, *366*, 576−585.
(14) Birkert, O.; Tünnemann, R.; Jung, G.; Gauglitz, G. *Anal. Chem.* **2002**, *74*, 834−840.
(15) Belge, G.; Beyerlein, D.; Betsch, C.; Eichhorn, K. J.; Gauglitz, G.; Grundke, K.; Voit, B. *Anal. Bioanal. Chem.* **2002**, *374*, 403−411.
(16) Gauglitz, G.; Brecht, A.; Kraus, G.; Mahm, W. *Sens. Actuators, B* **1993**, *11*, 21−27.
(17) Curtis, C. L.; Doan, V. V.; Credo, G. M.; Sailor, M. J. *J. Electrochem. Soc.* **1993**, *140*, 3492−3494.
(18) Lin, V. S. Y.; Motesharei, K.; Dancil, K. S.; Sailor, M. J.; Ghadiri, M. R. *Science* **1997**, *278*, 840−843.
(19) Masuda, H.; Fukuda, K. *Science* **1995**, *268*, 1466−1468.
(20) Masuda, H.; Hasegwa, F. J. *J. Electrochem. Soc.* **1997**, *144*, L127−L130.
(21) Masuda, H.; Yada, K.; Osaka, A. *Jpn. J. Appl. Phys.* **1998**, *37*, L1340−L1342.
(22) Nielsch, K.; Choi, J.; Schwirn, K.; Wehrspohn, R. B.; Gösele, U. *Nano Lett.* **2002**, *2*, 677−680.
(23) Lee, W.; Park, J. S. *Chem. Rev.* **2014**, *114*, 7487−7556.
(24) Santos, A.; Kumeria, T.; Losic, D. *TrAC, Trends Anal. Chem.* **2013**, *44*, 25−38.
(25) Santos, A.; Kumeria, T.; Losic, D. *Materials* **2014**, *7*, 4297−4320.
(26) Kumeria, T.; Santos, A.; Losic, D. *Sensors* **2014**, *14*, 11878−11918.
(27) Santos, A.; Balderrama, V. S.; Alba, M.; Formentín, P.; Ferré-Borrull, J.; Pallarès, J.; Marsal, L. F. *Adv. Mater.* **2012**, *24*, 1050−1054.
(28) Santos, A.; Kumeria, T.; Wang, Y.; Losic, D. *Nanoscale* **2014**, *6*, 9991−9999.
(29) Santos, A.; Kumeria, T.; Losic, D. *Anal. Chem.* **2013**, *85*, 7904−7911.
(30) Chen, Y.; Santos, A.; Wang, Y.; Kumeria, T.; Wang, C.; Li, J.; Losic, D. *Nanoscale* **2015**, *7*, 7770−7779.
(31) Kumeria, T.; Rahman, M. M.; Santos, A.; Ferré-Borrull, J.; Marsal, L. F.; Losic, D. *Anal. Chem.* **2014**, *86*, 1837−1844.
(32) Chen, Y.; Santos, A.; Wang, Y.; Kumeria, T.; Ho, D.; Li, J.; Wang, C.; Losic, D. *Sci. Rep.* **2015**, *5*, 12893.
(33) Nemati, M.; Santos, A.; Kumeria, T.; Losic, D. *Anal. Chem.* **2015**, *87*, 9016−9024.
(34) Kumeria, T.; Rahman, M. M.; Santos, A.; Ferré-Borrull, J.; Marsal, L. F.; Losic, D. *ACS Appl. Mater. Interfaces* **2014**, *6*, 12971−12978.
(35) Kumeria, T.; Santos, A.; Rahman, M. M.; Ferré-Borrull, J.; Marsal, L. F.; Losic, D. *ACS Photonics* **2014**, *1*, 1298−1306.
(36) Rahman, M. M.; Marsal, L. F.; Pallarès, J.; Ferré-Borrull. *ACS Appl. Mater. Interfaces* **2013**, *5*, 13375−13381.
(37) Chen, Y.; Santos, A.; Wang, Y.; Kumeria, T.; Li, J.; Wang, C.; Losic, D. *ACS Appl. Mater. Interfaces* **2015**, *7*, 19816−19824.
(38) Wang, Y.; Chen, Y.; Kumeria, T.; Ding, F.; Evdokiou, A.; Losic, D.; Santos, A. *ACS Appl. Mater. Interfaces* **2015**, *7*, 9879−9888.
(39) Chen, Y.; Santos, A.; Ho, D.; Wang, Y.; Kumeria, T.; Li, J.; Wang, C.; Losic, D. *Electrochim. Acta* **2015**, *174*, 672−681.
(40) Santos, A.; Yoo, J.; Rohatgi, C.; Kumeria, T.; Wang, Y.; Losic, D. *Nanoscale* **2016**, *8*, 1360−1373.
(41) Santos, A.; Formentín, P.; Ferré-Borrull, J.; Pallarès, J.; Marsal, L. F. *Mater. Lett.* **2012**, *67*, 296−299.
(42) Wang, Y.; Santos, A.; Evdokiou, A.; Losic, D. *Electrochim. Acta* **2015**, *154*, 379−386.
(43) Dronov, R.; Jane, A.; Shapter, J. G.; Hodges, A.; Voelcker, N. H. *Nanoscale* **2011**, *3*, 3109−3114.
(44) Kumeria, T.; Losic, D. *Nanoscale Res. Lett.* **2012**, *7*, 88.
(45) Jani, A. M. Md.; Kempson, I. M.; Losic, D.; Voelcker, N. H. *Angew. Chem., Int. Ed.* **2010**, *49*, 7933−7937.
(46) Kumeria, T.; Santos, A.; Losic, D. *ACS Appl. Mater. Interfaces* **2013**, *5*, 11783−11790.
(47) Santos, A.; Montero-Moreno, J. M.; Bachmann, J.; Nielsch, K.; Formentín, P.; Ferré-Borrull, J.; Pallarès, J.; Marsal, L. F. *ACS Appl. Mater. Interfaces* **2011**, *3*, 1925−1932.
(48) Montgomery, D. C. *Design and Analysis of Experiments*, 5th ed.; John Wiley & Sons Inc.: New York, 2001.
(49) Abràmoff, M. D.; Magalhaes, P. J.; Ram, S. J. *Biophotonics Int.* **2004**, *11*, 36−42.
(50) Pacholski, C.; Sailor, M. J. *Phys. Status Solidi C* **2007**, *4*, 2088−2092.

DOI: 10.1021/acs.analchem.6b00993
Anal. Chem. XXXX, XXX, XXX−XXX